Appendix A — Maps of the potential global distribution of Citrus Black Spot

Maps of the potential distribution of Citrus Black Spot produced in Chapter 6 (published as Paul et al., (2005)) relied on a climate data base represented by weather data localities. Unfortunately, on a global scale, this database is not comprehensive. For example there were no climate data localities in Bhuthan and only two in Taiwan. In this appendix, the CLIMEX model of Chapter 6 is applied to a 0.5° gridded climate dataset developed by New et al. (1999). The gridded climate dataset includes climate data for Bhutan and Taiwan; and, in line with field observations, the map produced suggests that parts of these countries are suitable for disease establishment.

The gridded dataset represents mean monthly surface climate over land areas of the globe between 1961 and 1990. The data were interpolated from weather station data to a 0.5 degree latitude and longitude grid. Variables are precipitation and wet-day frequency, mean temperature, diurnal temperature range, vapour pressure, sunshine, cloud cover, ground frost frequency and windspeed. The data is fully described in New et al. (1999) and can be obtained from the IPPC Data Distribution Centre (http://ipcc-ddc.cru.uea.ac.uk).

Six maps are presented that indicate the climatic potential for CBS to establish in the main citrus growing regions of the world (compare with the maps of citrus growing regions in Chapter 2). Climatic potential is measured using an Ecoclimatic Index (EI): EI ≤ 4, climate unfavourable for the persistence of the species; 5 ≤ EI ≤10, marginally suitable for disease development; EI ≥ 11, favourable for disease development; and EI > 20, highly favourable for the persistence of CBS (Paul et al., 2005).

New, M., Hulme, M. & Jones, P. (1999) Representing twentieth-century space-time climate variability. Part I: Development of a 1961–90 mean monthly terrestrial climatology. Journal of Climate, 12, 829-856.

Paul, I., van Jaarsveld, A. S., Korsten, L. & Hattingh, V. (2005) The potential global geographical distribution of Citrus Black Spot caused by *Guignardia citricarpa* (Kiely): likelihood of disease establishment in the European Union. Crop Protection, 24, 297-308.

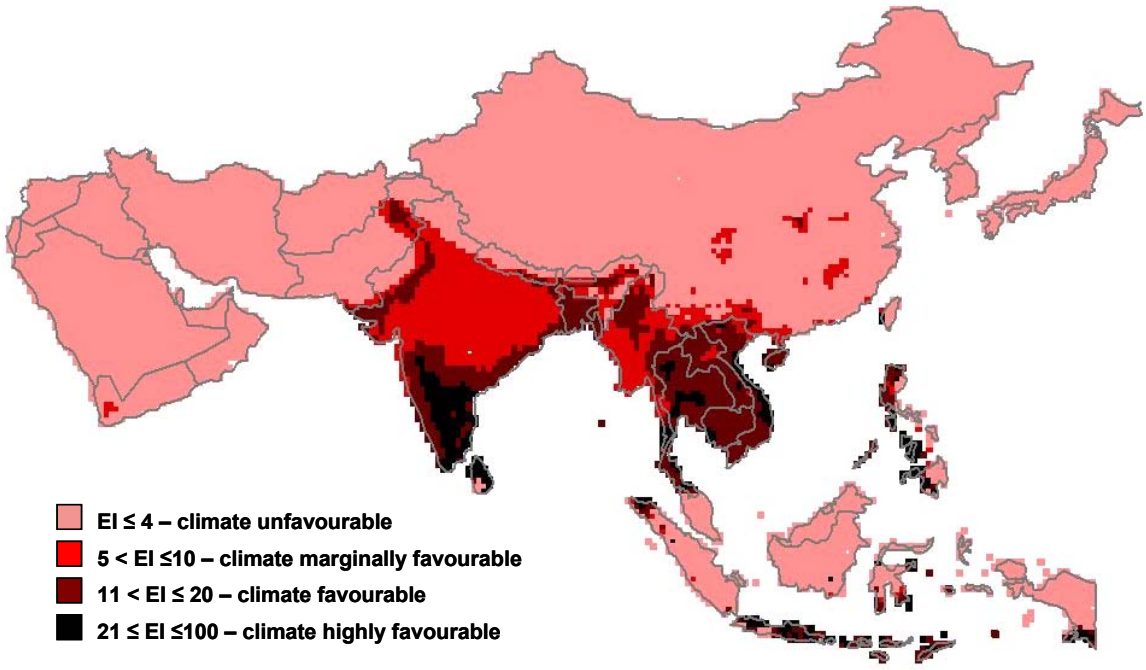

Figure A.1 — The climatic suitability of Asia for the occurrence of Citrus Black Spot.

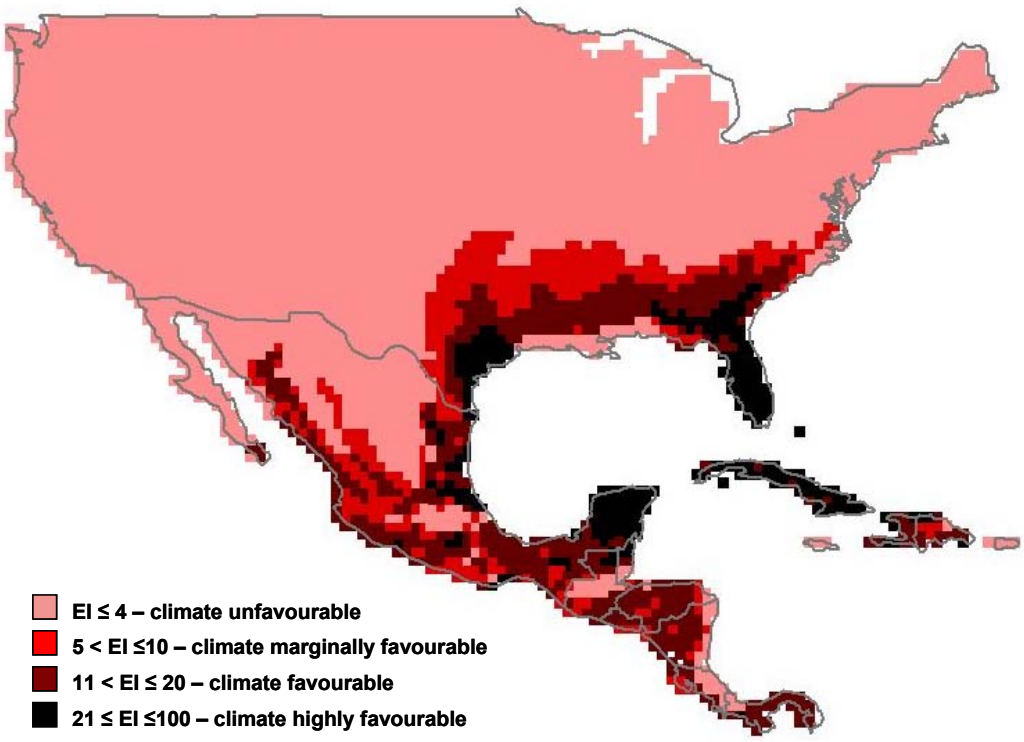

Figure A.2 — The climatic suitability of North and Central America for the establishment of Citrus Black Spot.

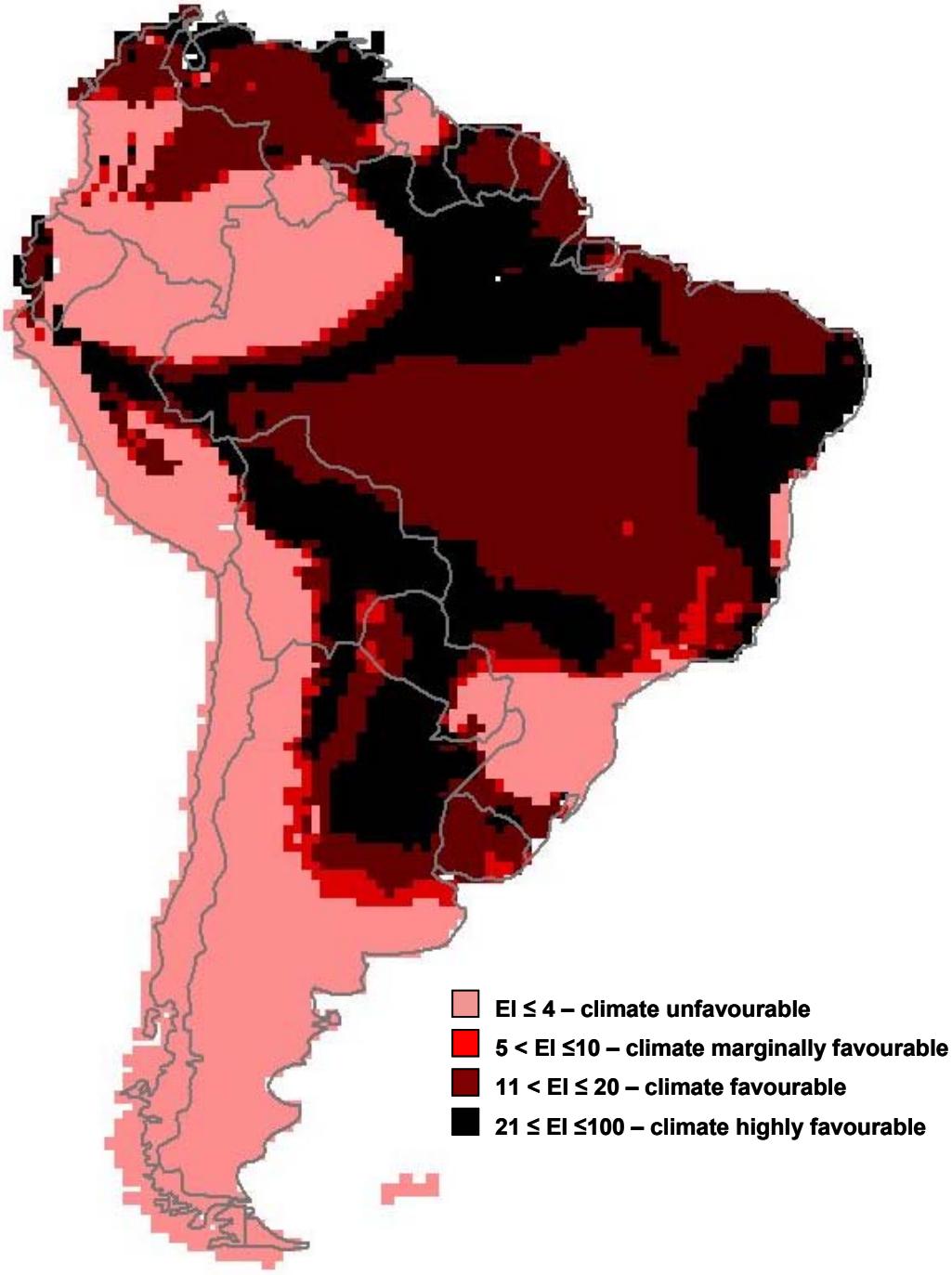

Figure A.3 — The climatic suitability of South America for the occurrence of Citrus Black Spot.

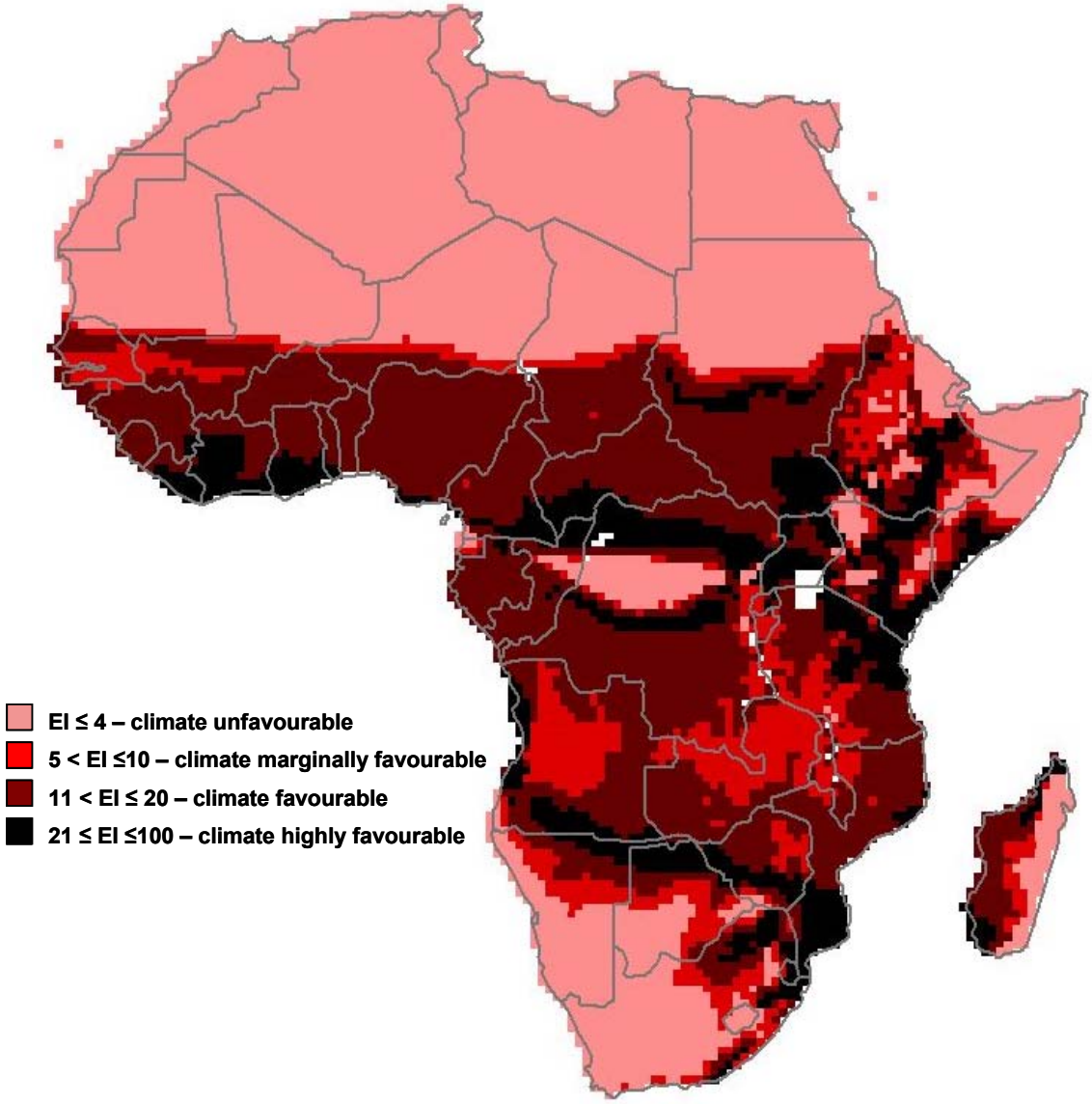

Figure A.4 — The climatic suitability for Africa for the occurrence of Citrus Black Spot.

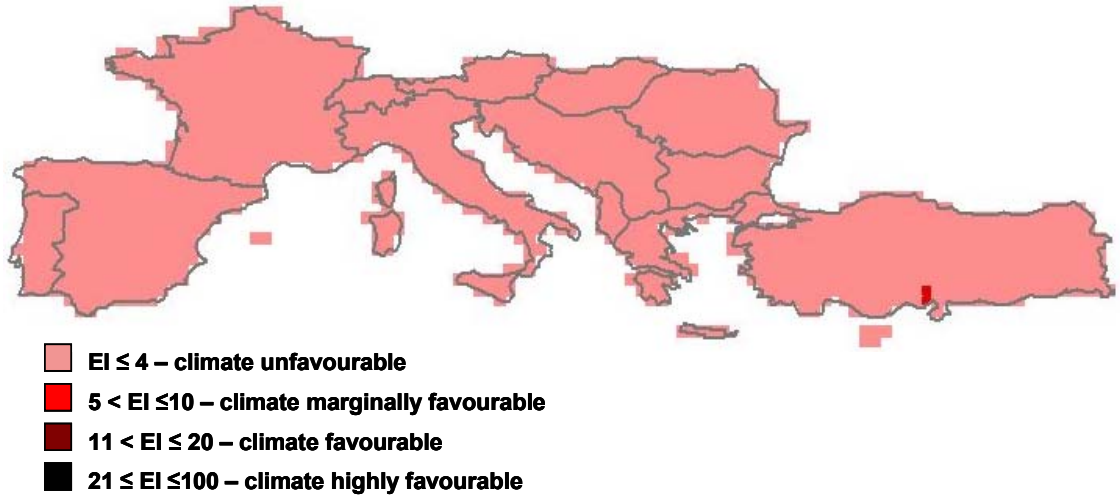

Figure A.5 — The climatic suitability of Southern Europe and Asia minor for the occurrence of Citrus Black Spot.

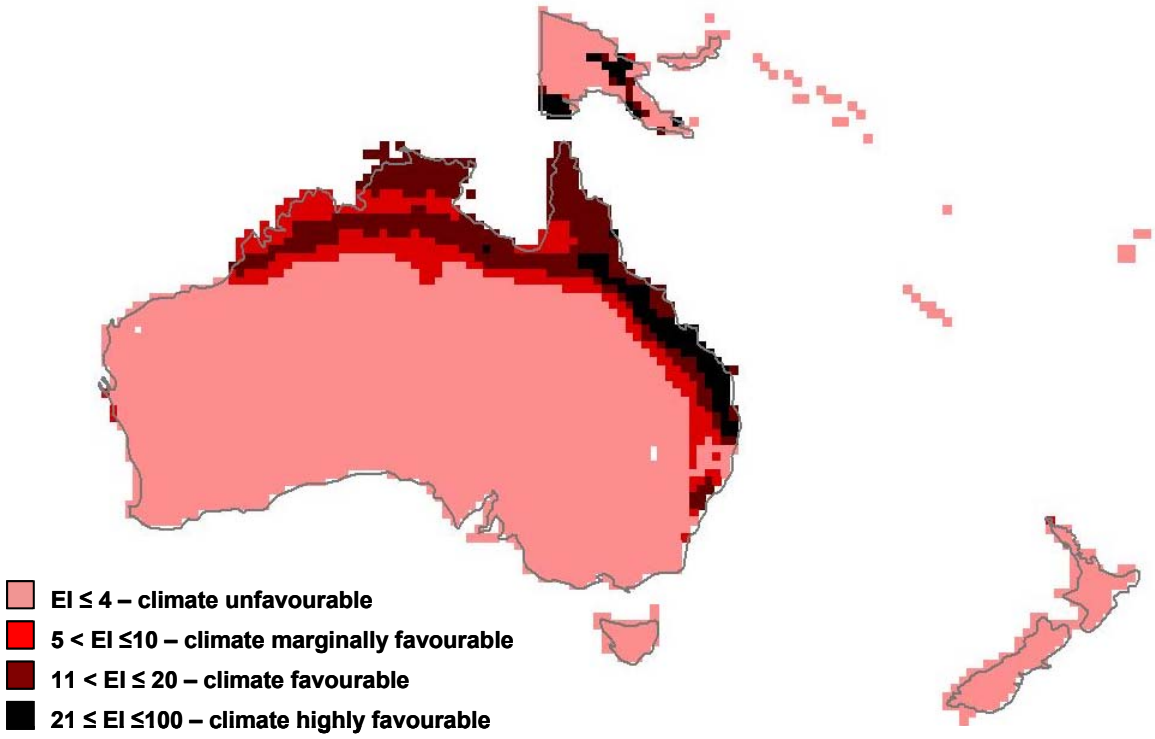

Figure A.6 — The climatic suitability of Oceania for the occurrence of Citrus Black Spot.

Appendix B — Differences between the SCT and Cramer data

Two climate data sets were used in this study. The Cramer data set, for which climate data were collated over the period of 1931–1960, and the SCT data set, for which climate data were collated over the period of 1961–1990. Data for both data sets used originate from direct measurements from weather data stations over the period that the data set relates to. The climate data were spatially interpolated. The Cramer data were spatially interpolated to the mean elevation values (calculated as the mean of the modal elevations) and the SCT data were obtained as values already spatially interpolated to minimum elevation values. Thus the climate data differed in the period in which the data were collated and in the elevation data to which the climate values were interpolated.

These climate data were used to calculate the bioclimate variable values for a 15' grid of South Africa that contained 1974 cells. The bioclimate variables were mean temperature of the coldest month (MTCO), mean temperature of the warmest month (MTWA) and the ratio of actual to potential evapotranspiration (AET/PET). However, differences in the climate data resulted in different values calculated for the bioclimate variables as can be seen from the maps of the bioclimate variable values. Maps of the bioclimate variable under climate change are also presented. Differences between the future climates are analysed in Appendix C.

AET/PET values above 0.9 were calculated from the Cramer data, but not from the SCT data (compare Figure B.1 and Figure B.2). Generally, MTCO and MTWA values from the SCT data are higher than from the Cramer data (compare Figure B.5 with Figure B.6, and Figure B.9 with Figure B.10). The MTCO values for the eastern coastal areas of South Africa are higher when calculated from the SCT data than when calculated from the Cramer data. Similarly, MTWA values for the area of the Kgalagadi Transfrontier Park (Northern Cape) as calculated from the SCT data are higher than those calculated from the Cramer data.

When modelling the potential distributions of species, the most appropriate climate data set should be chosen. The climate of Africa is warmer now than it was 100 years ago, and this warming has been particularly apparent since the 1970s. The six warmest years on record are all more recent than 1987, with 1998 being the warmest (Hulme et al., 2001). This recent rise in temperature is not captured by the Cramer climate data, as these data were collected between 1931–1960. Because of this, although the Cramer data were interpolated from more data localities than the SCT data, the SCT data are accepted to be more reliable for modelling the potential distribution of citrus and CBS.

Hulme, M., Doherty, R., Ngara, T., New, M. & Lister, D. (2001) African Climate Change: 1900–2100. Climate Research, 17, 145-168.

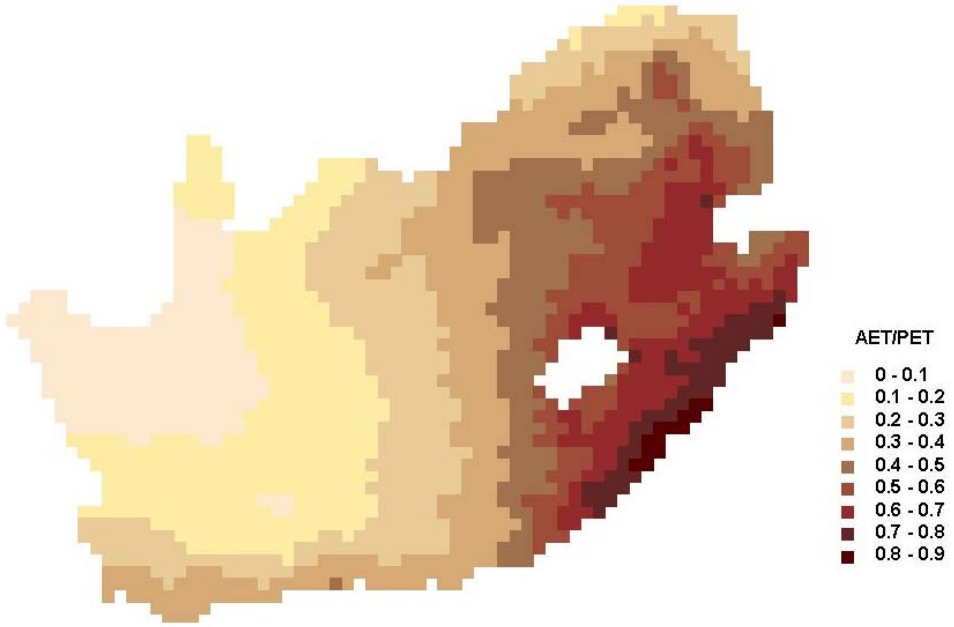

Figure B.1 — The ratio of actual to potential evapotranspiration (AET/PET), SCT data.

Figure B.2 — The ratio of actual to potential evapotranspiration (AET/PET), Cramer data

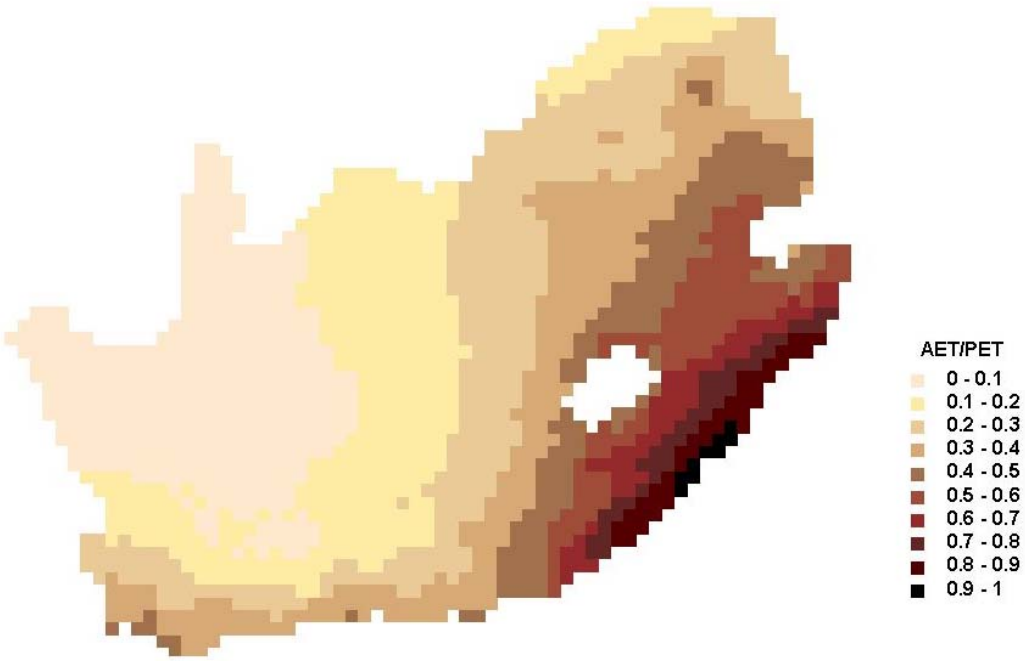

Figure B.3 — The ratio of actual to potential evapotranspiration (AET/PET) values calculated for the SCT data using the future climate represented by the HadCM3 B2 scenario.

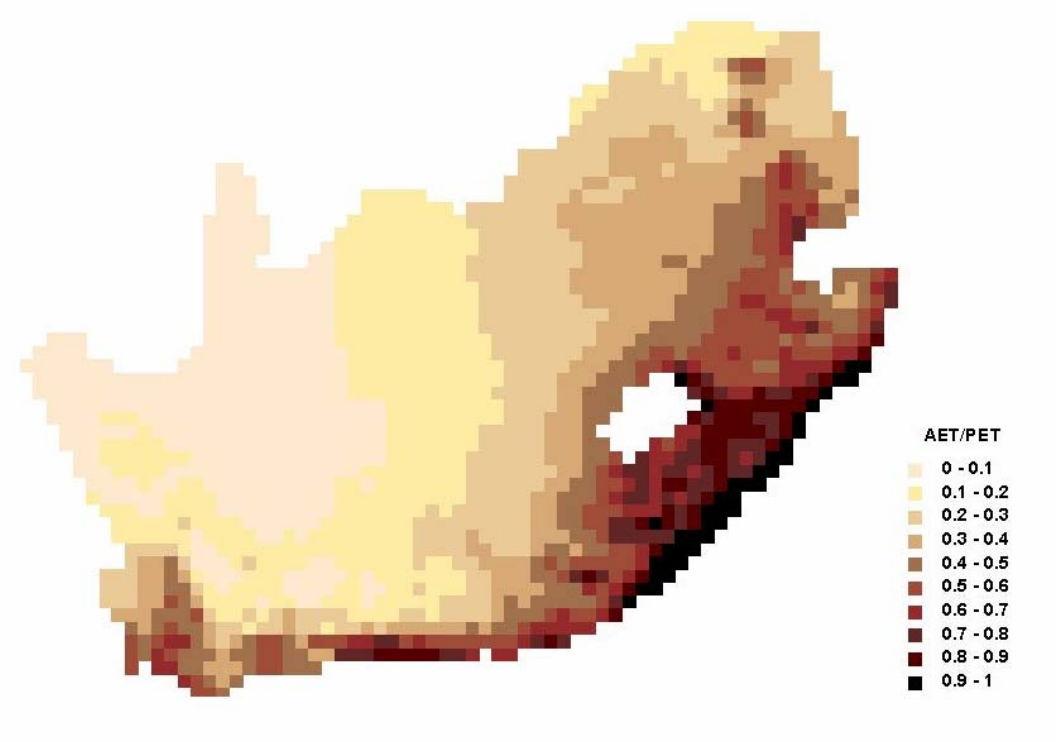

Figure B.4 — The ratio of actual to potential evapotranspiration (AET/PET) values calculated for the Cramer data using the future climate represented by the HadCM3 B2 scenario.

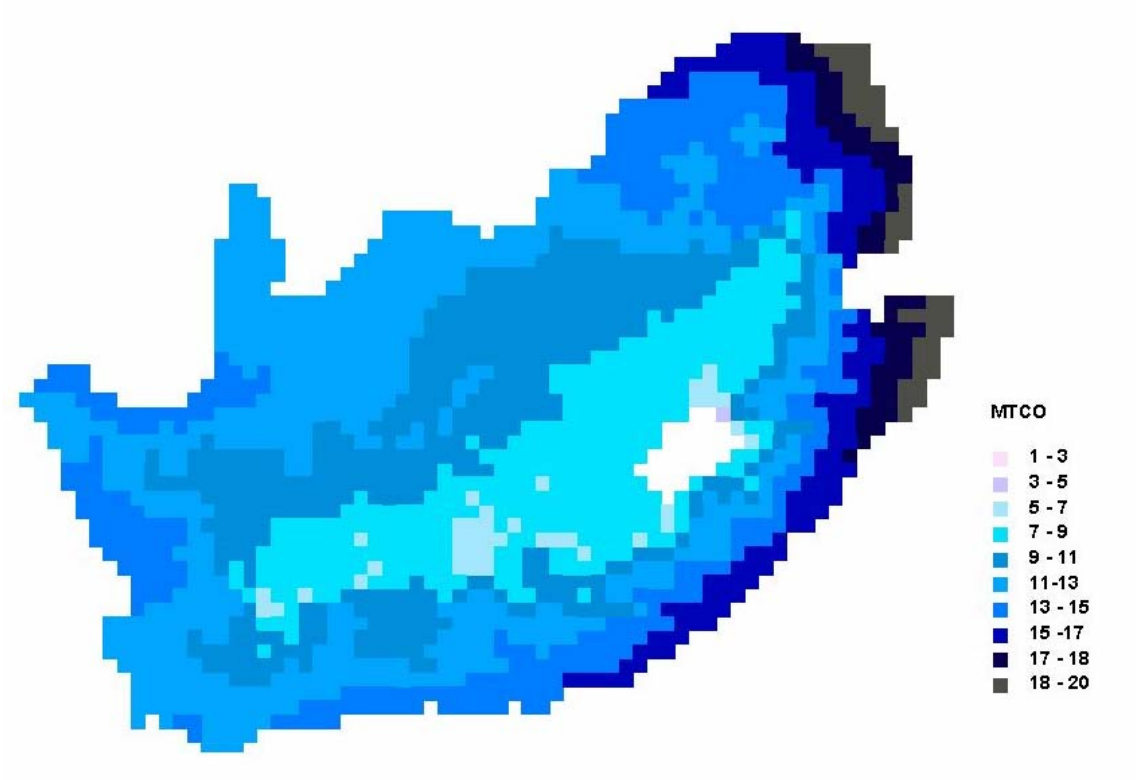

Figure B.5 — Mean temperature of the coldest month (°C), SCT data.

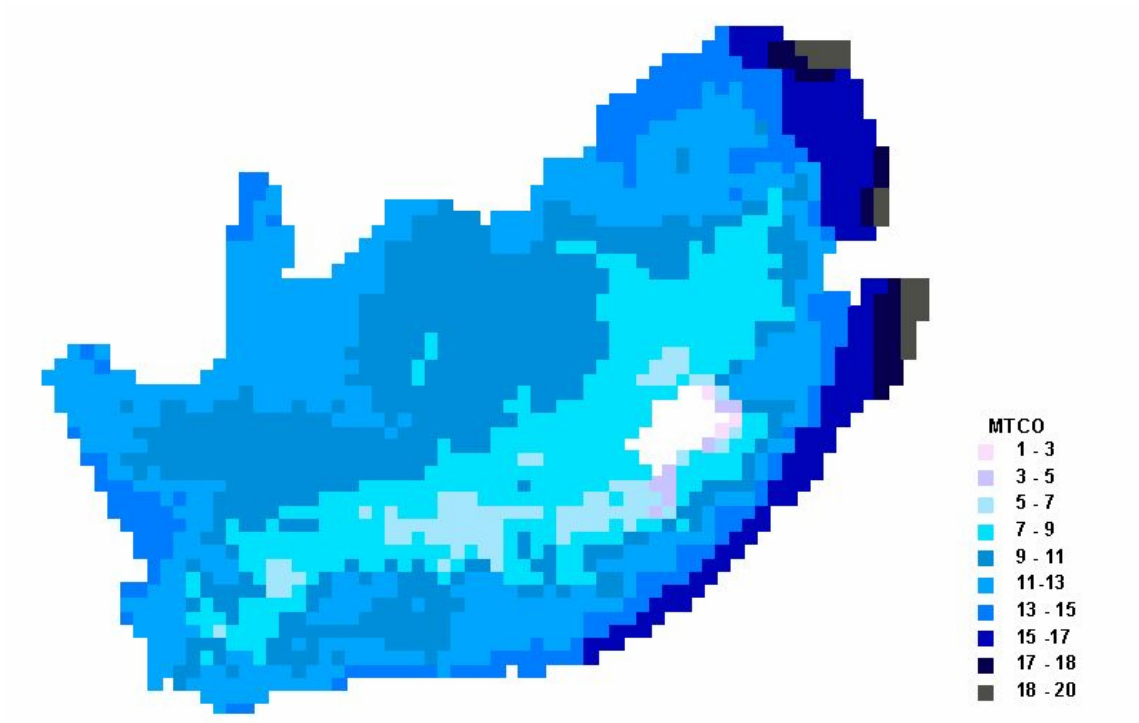

Figure B.6 — Mean temperature of the coldest month (°C), Cramer data.

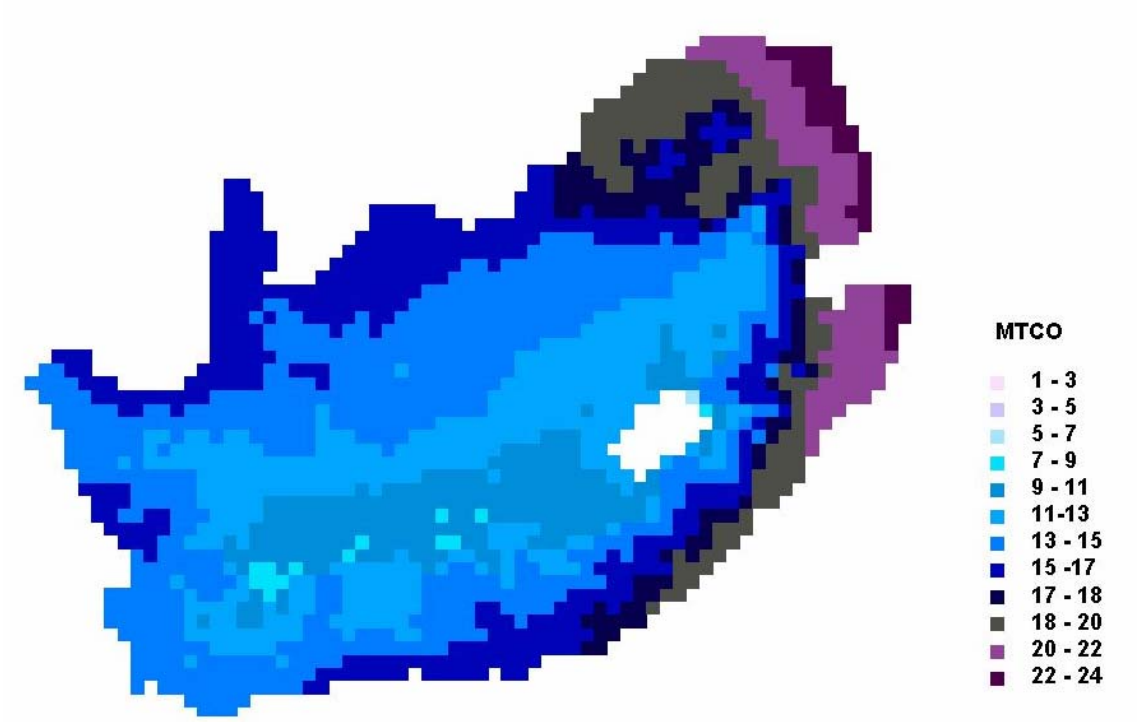

Figure B.7 — Mean temperature of the coldest month values (°C) calculated for the SCT data using the future climate represented by the HadCM3 B2 scenario.

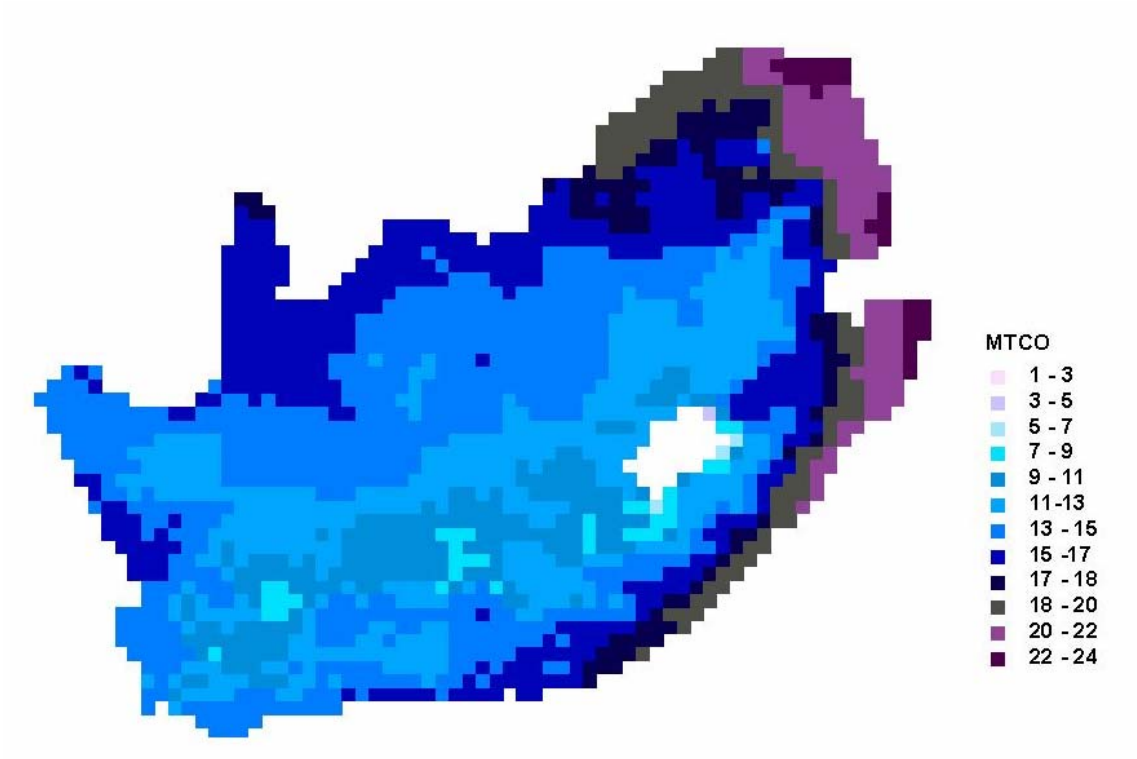

Figure B.8 — Mean temperature of the coldest month (°C) values calculated for the Cramer data using the future climate represented by the HadCM3 B2 scenario.

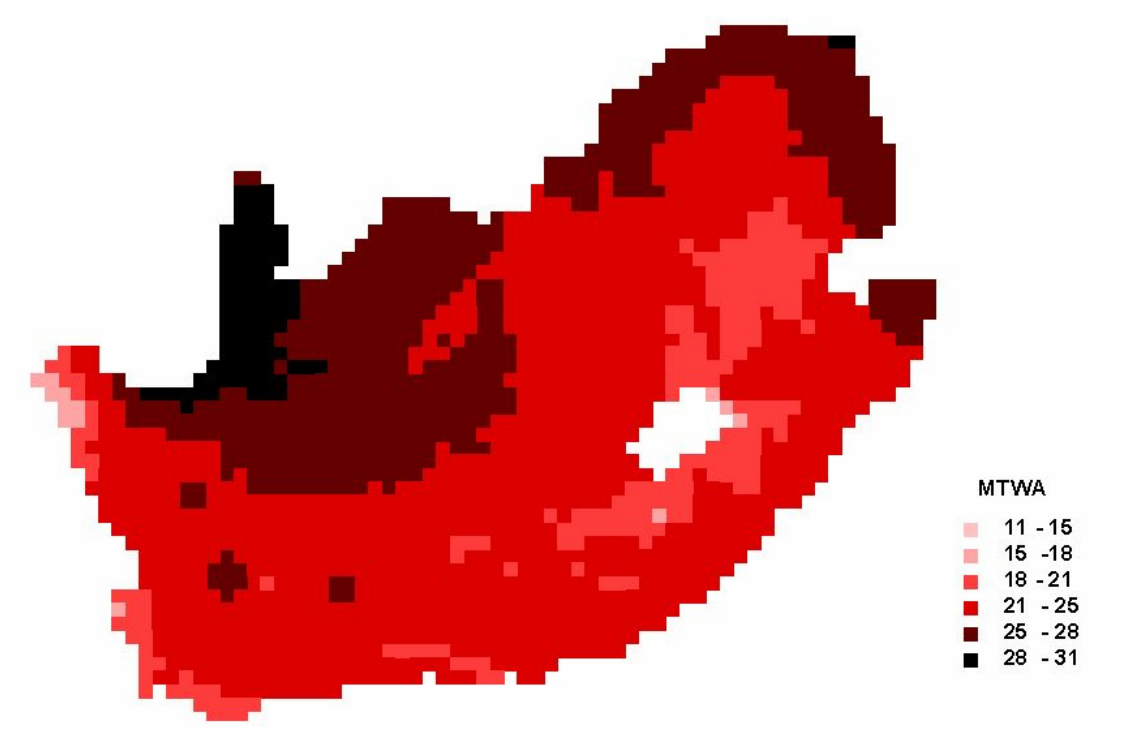

Figure B.9 — Mean temperature of the warmest month (°C), SCT data.

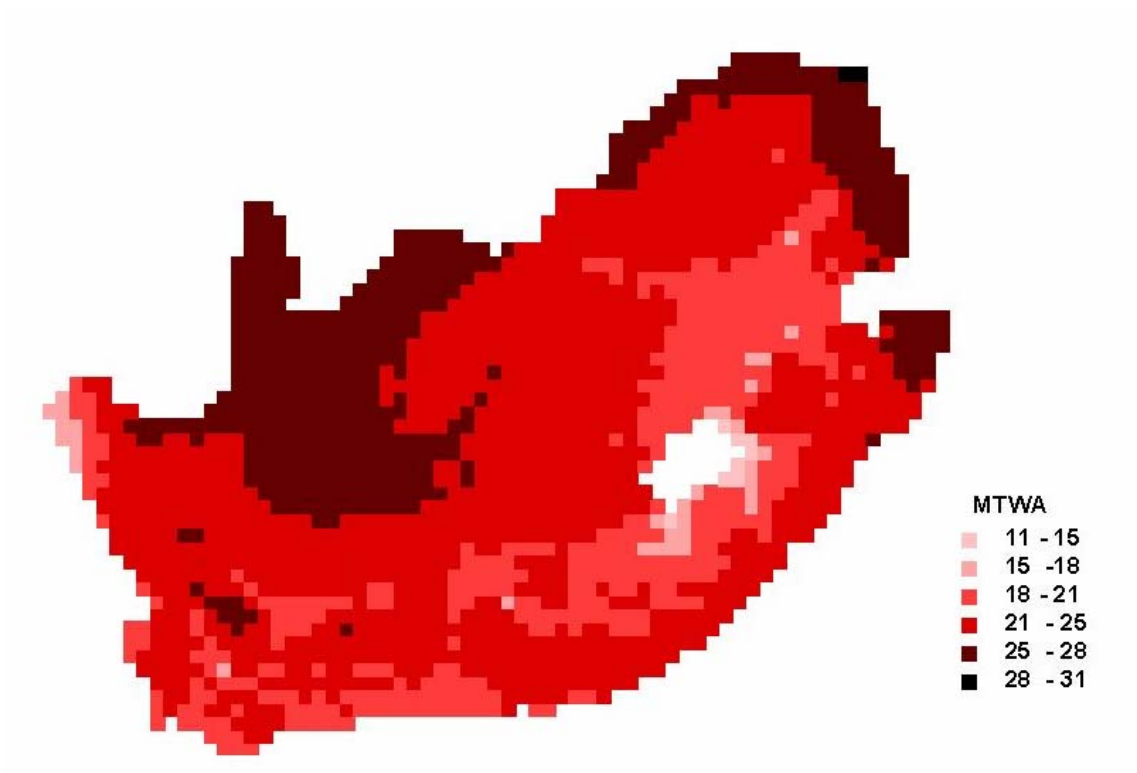

Figure B.10 — Mean temperature of the warmest month (°C), Cramer data.

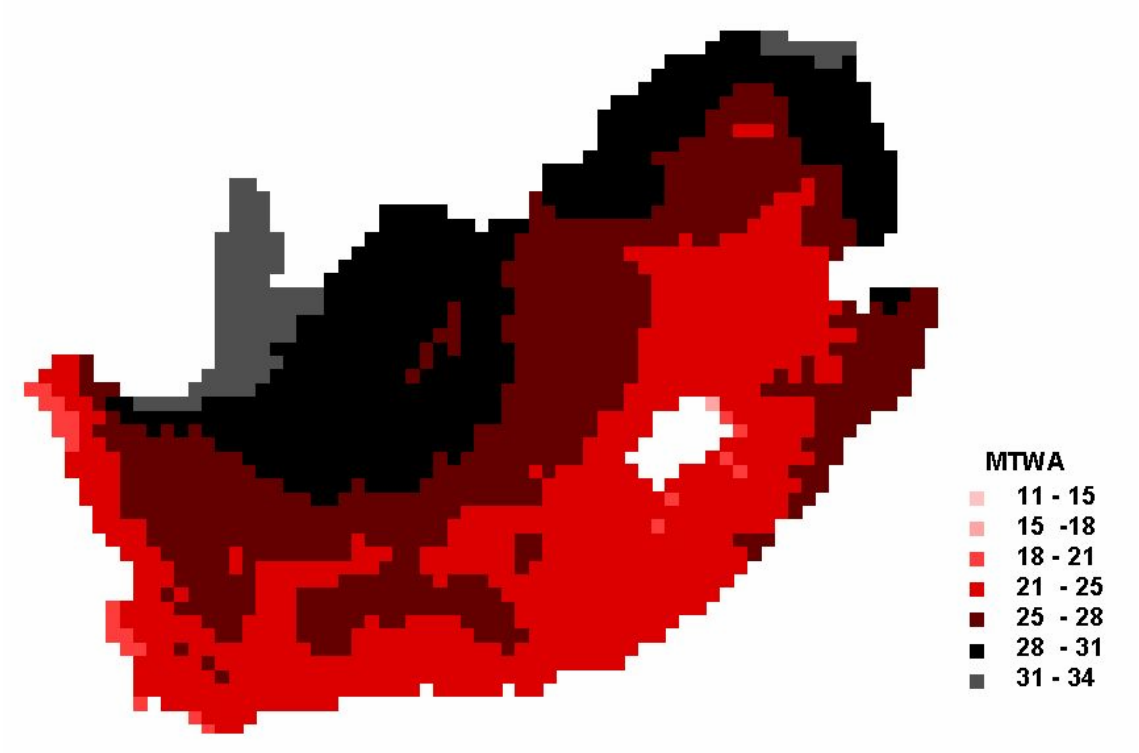

Figure B.11 — Mean temperature of the warmest month values (°C) values calculated for the SCT data using the future climate represented by the HadCM3 B2 scenario.

Figure B.12 — Mean temperature of the warmest month (°C) values calculated for the Cramer data using the future climate represented by the HadCM3 B2 scenario.

Appendix C — Potential future climate of South Africa

The nature of the simulated change in climate for South Africa is illustrated by mapping areas of projected future climates that are analagous to the current climate.

Future climates were compared to records seen as representative of current climate. This was done for both the SCT data (1961–1990) and the Cramer data (1931–1960). Comparisons were based on the values for three bioclimate variables, namely the mean temperature of the coldest month (MTCO); the mean temperature of the warmest month (MTWA); and the ratio of actual to potential evapotranspiration (AET/PET).

So that the variables had equal weight when they were compared, the variables were standardised using the standard normal,

$$A_x' = \frac{A_x - \bar{\bar{A}}}{\sigma_A} \qquad 1$$

where A_x' is the standardised value of a bioclimate variable A at grid cell x; A_x is the value of bioclimate variable A at grid cell x; $\bar{\bar{A}}$ is the mean of all values (current and future) of bioclimate variable A; and σ_A is the standard deviation of all values (current and future) of bioclimate variable A.

As the AET/PET values represent proportions, AET/PET values were linearised using the logit transformation before being standardised. The logit transformation is,

$$x' = \ln\left(\frac{x}{1-x}\right) \qquad 2$$

where x' is a transformed datum, and x is an original proportion datum. So that the logit transformation did not return infinite values, any untransformed AET/PET values of 1 were converted to 0.999.

Visual inspection confirmed that each standardised bioclimate variable approximated the normal distribution, with a mean of zero and standard deviation of one.

The climate at a grid cell could then be compared with the climate at another grid cell using the inversed square Euclidean distance. The Euclidean distance between two grid cells is calculated as,

$$d_{(i,j)} = \sqrt{\left(mtco_i' - mtco_j'\right)^2 + \left(mtwa_i' - mtwa_j'\right)^2 + \left(apet_i' - apet_j'\right)^2} \qquad 3$$

where $d_{(i,j)}$ is the Euclidean distance between the climate at grid cell i and the climate at grid cell j; A_i' is the value of environmental variable A at grid cell i (standardised using equation 2); and A_j' is the value of environmental variable A at grid cell j standardised using equation 2).

To measure how similar the projected future climate is to the current climate the minimum Euclidean distance between a grid cell of the future climate and all the grid cells of the current climate was calculated. This calculation was done for all the grid cells within the future climate data. This comparison reveals where climates similar to the future climate may be found in South Africa today.

To quantitatively assess the minimum distances calculated for future grid cells, current climate was also compared by calculating the minimum Euclidean distance between at a grid cell of the current climate and all the other grid cells of the current climate. The minimum Euclidian distances obtained from these calculations were well described by a log-normal distribution. Therefore, the likelihood that the climate at a future grid cell would be similar to the current climates could be calculated from the expected distribution of the calculated minimum distance values. Figure C.1 (SCT data) and Figure C.2 (Cramer data) show the degree of similarity between the future climates and the observed current climates in South Africa.

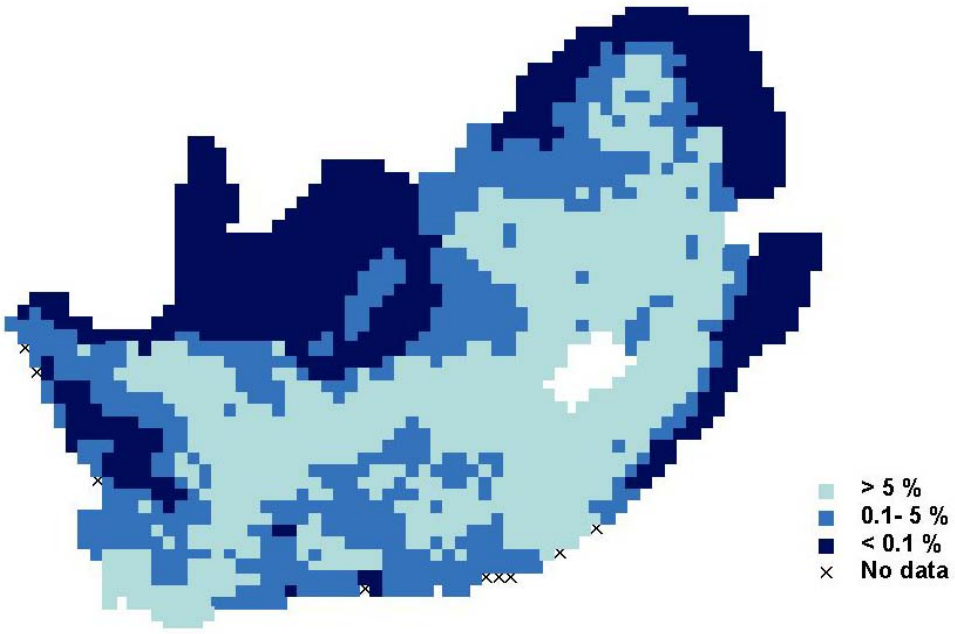

Figure C.1 — A grid of South Africa indicating the similarity between future and current climate using SCT data. The liklihoods that the future climate at grid cells are represented somewhere in the current climate of South Africa are shown.

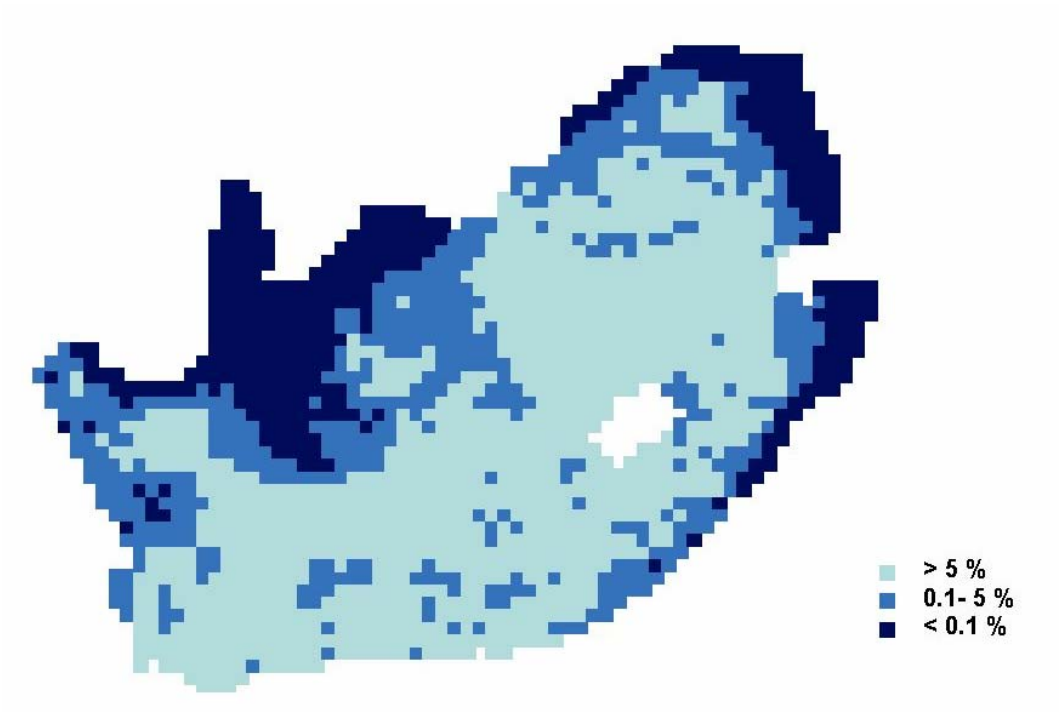

Figure C.2 — A grid of South Africa indicating the similarity between future and current climate using Cramer data. The liklihoods that the future climate at grid cells are represented somewhere in the current climate of South Africa are shown.

For the SCT data and the Cramer data a future climate analogous to the current climate in South Africa is predicted for most of the interior of the country. Climates along the Eastern and Western coastlines and also against the Northern borders of the country and notably the greatest parts of the Northern Cape are calculated to be different from present climates.

Figure C.1 and Figure C.2, however, do not show which current areas in South Africa are most similar to the future climates, or which currently observed climates are no longer represented in the future climates. This is shown in Figure C.3 and

Figure C.4, where the frequency with which the observed climate at a grid cell was found to be closest (most similar) to future climate was plotted for the SCT and the Cramer data respectively. For both the SCT and Cramer data the pattern shows that future climates are not well represented by inland climates. Particularly high frequencies of future aligned climates were found along the northern borders of the country.

To verify that these patterns are not an artefact of the occurrence of current climates, the procedure was repeated to identify the frequency with which the current climate at a grid cell was found to be similar to other grid cells across the country. In this case, using the SCT data set as an example, climates were much more evenly distributed across South Africa, with a large number of grid cells only having four other cells with similar climates from across the region (Figure C.5). This is in contrast to the comparison with future climates where over thirty grid cells had ten of more grid cells with similar climates. This means that the current climates are relatively heterogeneous across the landscape but that future climates are likely to have a broader distribution (higher frequency).

The changes in climate can also be visualised by comparing maps of the bioclimate variable values as calculated for the current climate data with those calculated for the future climate scenario (See Appendix B, Figure B.1–Figure B.12).

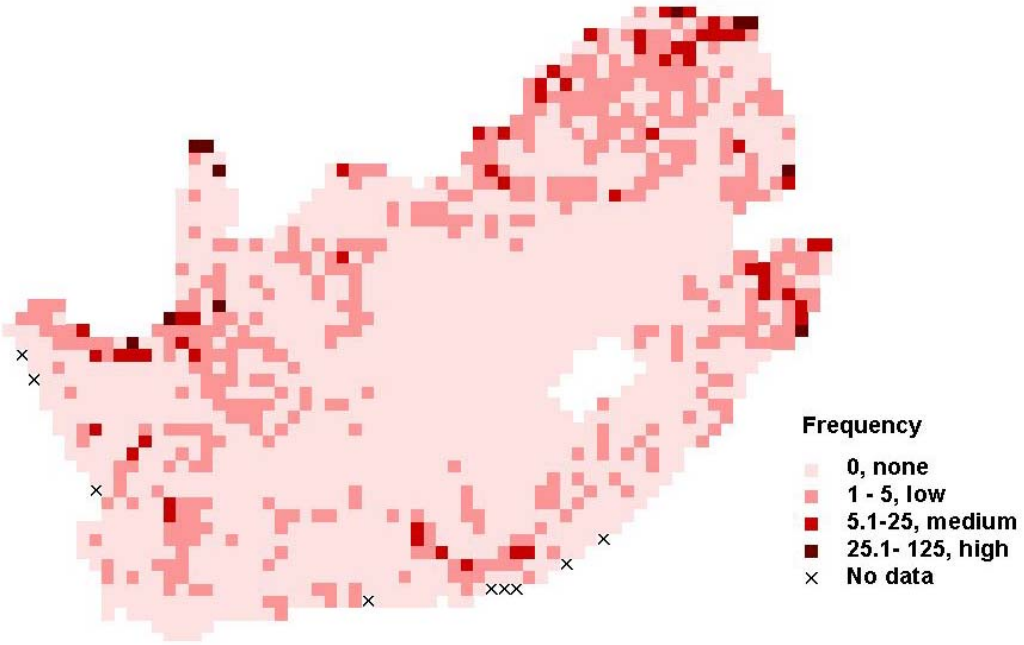

Figure C.3 — A grid map of South Africa indicating those grid cells that were most frequently similar to a future grid cell, SCT data. The different categories refer to the number of grid cells from the future climates with similar climates.

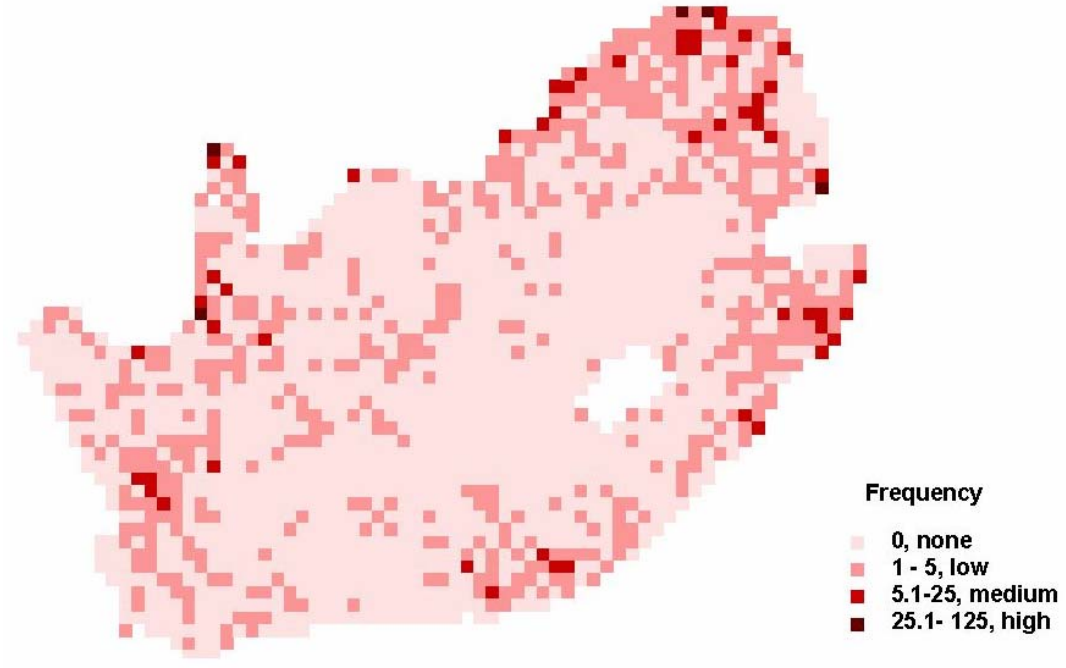

Figure C.4 — A grid map of South Africa indicating those grid cells that were most similar to future grid cells, Cramer data. The different categories refer to the number of grid cells from future climate with similar climates.

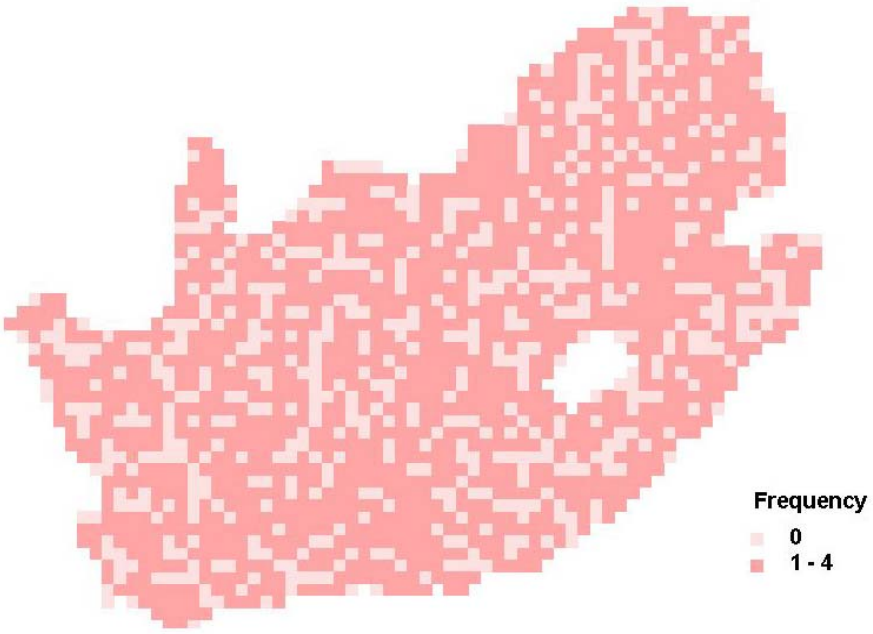

Figure C.5 — A grid of South Africa showing the frequency with which a single grid cell was used to explain the climate of other grid cells, when measuring the similarity of current climate to itself.

Appendix D — Flow diagram of the potential direct and indirect impacts of climate change on crops and pathogens

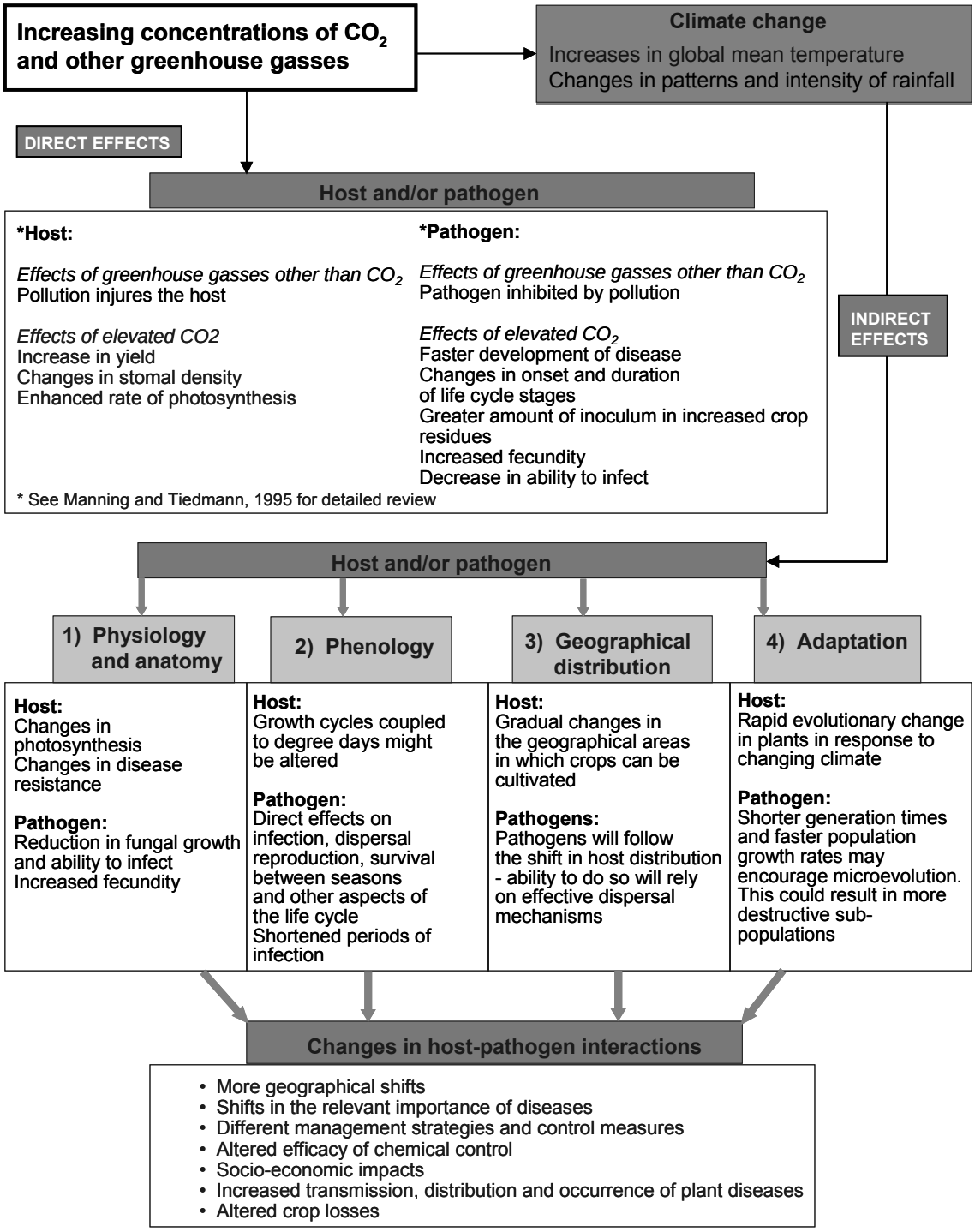

Bone, E. & Farres, A. (2001) Trends and rates of microevolution in plants. Genetica, 112-113, 165-182.

Chakraborty, S. & Datta, S. (2003) How will plant pathogens adapt to host resistance at elevated CO2 under a changing climate? New Phytologist, 159, 733-742.

Chakraborty, S., Murray, G. & White, N. (2002) Impact of climate change on important plant diseases in Australia, Report: WO2/010/. Rural industries research and development co-operation, Kingston, Australia.

Chakraborty, S., Murray, G. M., Magarey, P. A., Yonow, T., O'Brien, R. G., Croft, B. J., Barbetti, M. J., Sivasithamparam, K., Old, K. M., Dudzinski, M. J., Sutherst, R. W., Penrose, L. J., Archer, C. & Emmett, R. W. (1998) Potential impact of climate change on plant diseases of economic significance to Australia. Australasian Plant Pathology, 27, 15-35.

Coakley, S. M., Scherm, H. & Chakraborty, S. (1999) Climate change and plant disease management. Annual Review of Plant Pathology, 37, 399-426.

Manning, W. J. & Tiedmann, A. V. (1995) Climate change and the potential effects of increased atmospheric carbon dioxide (CO2), ozone (O3) and Ultraviolet-B (UV-B) radiation on plant diseases. Environmental Pollution, 88, 219-245.

Scherm, H. & Coakley, S. M. (2003) Plant pathogens in a changing world. Australasian Plant Pathology, 32, 157-165.